Hindawi Publishing Corporation
Journal of Sensors
Volume 2008, Article ID 782764, 7 pages
doi:10.1155/2008/782764

Research Article

Micro-Optoelectromechanical Tilt Sensor

Timothy G. Constandinou[1, 2] and Julius Georgiou[1]

[1] *Holistic Electronics Research Lab, ECE Department, University of Cyprus, 1678 Nicosia, Cyprus*
[2] *Institute of Biomedical Engineering, Imperial College London, London SW7 2AZ, UK*

Correspondence should be addressed to Timothy G. Constandinou, t.constandinou@imperial.ac.uk

Received 19 February 2008; Accepted 19 April 2008

Recommended by Ignacio Matias

This paper presents a novel hybrid CMOS/MEMS tilt sensor with a 5° resolution over a 300° range. The device uses a MEMS-based semicircular mass suspended from a rigid body, projecting a shadow onto the CMOS-based optical sensor surface. A one-dimensional photodiode array arranged as a uniformly segmented ring is then used to determine the tilt angle by detecting the position of the semicircular mass. The complete sensor occupies an area of under 2.5 mm × 2.5 mm.

1. INTRODUCTION

An increasing number of medical devices including implantable prosthetics and body worn instrumentation are incorporating sense systems within and around the body. Physical constraints demand such devices to be compact and lightweight, and the need for autonomy imposes stringent power budgets on such systems. One such sensor is the *inclinometer* (or tilt sensor), which senses its orientation with respect to gravity.

Sensing tilt, in personalised medicine is becoming increasingly important, especially when combined with other sensor modalities. For example, a tilt sensor incorporated within a heart monitor can provide a metric on the patients' activity, providing additional insights for interpreting the electrocardiogram data. In other biomedical applications, real-time, accurate tilt data can be used in therapy, for example, in correcting vestibular balance disorders.

The vast majority of tilt sensors developed to date are capacitive (or conductive) in nature, often with electrolytic fluid-filled cavities. Such systems have been developed by Bretterklieber et al. [1] and more recently using MEMS technology [2, 3]. Zhao and Yeatman [4] have developed a *digital* MEMS-based tilt sensor offering the possibility of simplifying the interface electronics. It has also been reported possible to implement inclinometers using modified accelerometers [5, 6] but such systems are typically limited in range and/or sensitivity. Other approaches include a MEMS convection-based [7] and optical microfilter-based [8] tilt sensors.

In this paper, we present a novel ultra-low-power tilt sensor generating a digital output. This has been implemented as part of a hybrid two-chip solution (MEMS microstructure/CMOS vision chip) and has been fabricated.

2. SYSTEM ARCHITECTURE AND CIRCUIT IMPLEMENTATION

This tilt sensor uses a micromechanical semicircular mass to express the gravitational field optically and then custom CMOS vision chip to detect and resolve the vector. This concept is illustrated in Figure 1.

The design splits the 330° field of view into two 165° half-planes, which we have chosen to refer to as left- and right-hand-side (LHS, RHS) horizons. This is illustrated in the top-level system architecture, shown in Figure 2. As the micromechanical semicircular mass moves, it forms a shadow that is projected onto the surface of the CMOS chip, the edge of which crosses both the LHS and RHS horizons. Therefore, each *horizon detector* is required to sense the position (or tilt angle) of these edges. By taking the difference, the output can encode the tilt angle using a signed, digital representation.

3. HORIZON DETECTOR CIRCUIT

The circuit implementation of the half-plane horizon detectors is shown in Figure 3. This consists of 33 photodiode elements positioned equidistantly around an arc to detect the

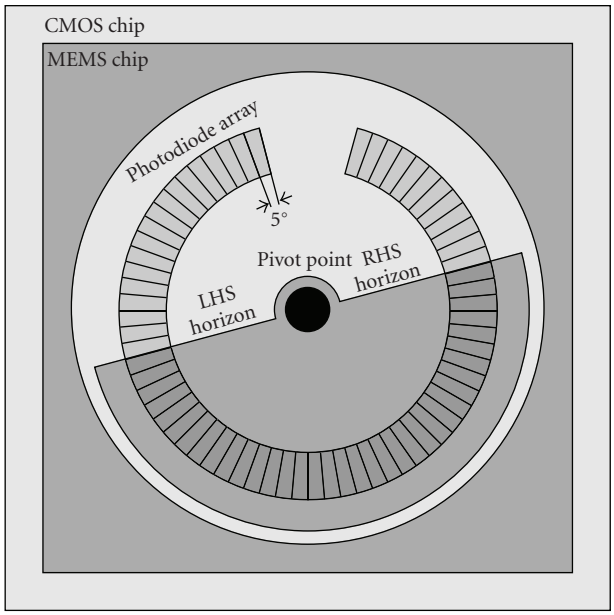

Figure 1: The micro-optoelectromechanical tilt sensor concept, based on a two-tier stack comprising of MEMS structure on top of CMOS die. The optical detector has 66 photodetector elements arranged in 5° segments to cover a 330° field-of-view (FOV).

position of the semicircular mass. Between each two adjacent photodiodes, we use a discrete edge detector element (that is in total, 32 edge detectors per horizon) to compare photocurrent magnitudes and if sufficiently different flag an edge-detect signal. The output is captured using a sequence of operations. Firstly, the address bus is initialised using pull-up devices to precharge the parasitic capacitance. Next, a *DRIVE* signal is propagated through the one-dimensional array, that is, 1×32 elements, until an edge signal is encountered. On detecting an edge condition, the current position is asserted onto the address bus via the address encoder, constituting (for each element) the relevant pull-down switches. Subsequently, the *DRIVE* signal is terminated and the address bus is sampled onto a 5-bit register.

4. EDGE DETECTOR CIRCUIT

Figure 4 shows the circuit schematic of the edge detector element. This has been adapted from Constandinou et al. [9, 10] to the expected contrast ratio and photocurrent levels. A global tuning mechanism is maintained by driving the I_{bias} and I_{tune} references off-chip and internally duplicating and distributing to the individual edge detector elements. The *DRIVEIN* and *DRIVEOUT* are used to test an individual edge detectors state before propagating to test the next element. Additionally, an artificial propagation delay is implemented within the output buffer to guarantee robustness.

5. PHOTODIODE DESIGN

The photodiodes are implemented using an n-well/p-substrate junction as illustrated in Figure 5. The different photodiode elements (66 devices) have been individually custom designed (to comply with design rule geometry) to fit within a 550 μm to 600 μm radius arc in 5° segments. The active sensor surface for each photodiode element comes to: 4245 μm^2. The photodiode is reverse-biased by stacking two diode-connected PMOS devices to Vdd. The photocurrent range for the given device under the expected light levels is from 1 pA (dark current) to 100 nA. The photodiode achieves a spectral responsivity of 0.15 A/W, 0.25 A/W, and 0.3 A/W for wavengths $\lambda = 475$ nm (blue), $\lambda = 510$ nm (green), and $\lambda = 630$ nm (red), respectively, when being uniformly illuminated at 5 μW/mm^2.

6. 4-PHASE CLOCK GENERATION CIRCUIT

The operation of the tilt sensor is centrally regulated via a 4-phase clock sequence, generated using the circuit shown in Figure 6. This implements a looping 4-element state machine to generate the required control signals. Phase actions are: $\varphi 1$ to precharge the bus, $\varphi 2$ to interrogate the LHS and RHS horizons and drive the bus, $\varphi 3$ to sample the bus result on horizon register, and $\varphi 4$ to sample the difference (i.e., subtraction) on the output register.

7. CMOS/MEMS INTEGRATED CIRCUITS

Figures 7 and 8 show the CMOS and MEMS microphotographs, respectively.

The MEMS component has been designed such that the pivot/axel used to suspend the mass is smooth and has little friction. In addition, we patterned the release holes in the semicircular mass with a specific pattern recommended by the Tronics foundry, which forms bumps which ensure that there is enough space between the main surface area and the sidewall to avoid stiction [11]. Furthermore, the mass includes antisticking holes to ensure release, based on technical data provided from Tronics foundry. During fabrication, the design incorporates a number of struts to secure the mass during processing and release. After manufacture, these struts have been intentionally designed to be breakable, thus releasing the semicircular mass into operation.

8. SIMULATION RESULTS

The circuit was simulated using the Cadence Spectre (5.1.41isr1) simulator with foundry supplied BSIM3v3 models. Parametric operating point simulations have been performed to determine the onset of edge detection for various bias conditions. These results are illustrated in Figure 9. The family of curves (for different values of I_{bias}) illustrates the minimum contrast ratio ($I_{\text{photo}}/\delta I_{\text{photo}}$) required to flag an edge detection condition. The tunability (for different values of I_{tune}) is represented in the y-axis variation. These results show main trends of operation: (i) for $I_{\text{bias}} < I_{\text{photo}}$ the tunable range is not significantly effected by bias current level, and (ii) for $I_{\text{bias}} > I_{\text{photo}}$, increasing the bias current level significantly increases the tunable range (in particular extending the contrast ratio). It therefore

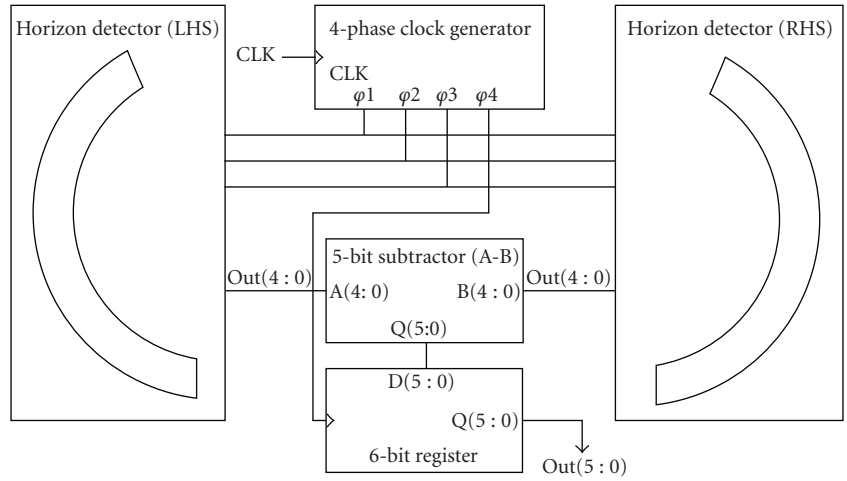

Figure 2: The top-level system architecture comprising of two half-plane horizon detectors, clock phase generator, and 2's compliment subtraction circuit.

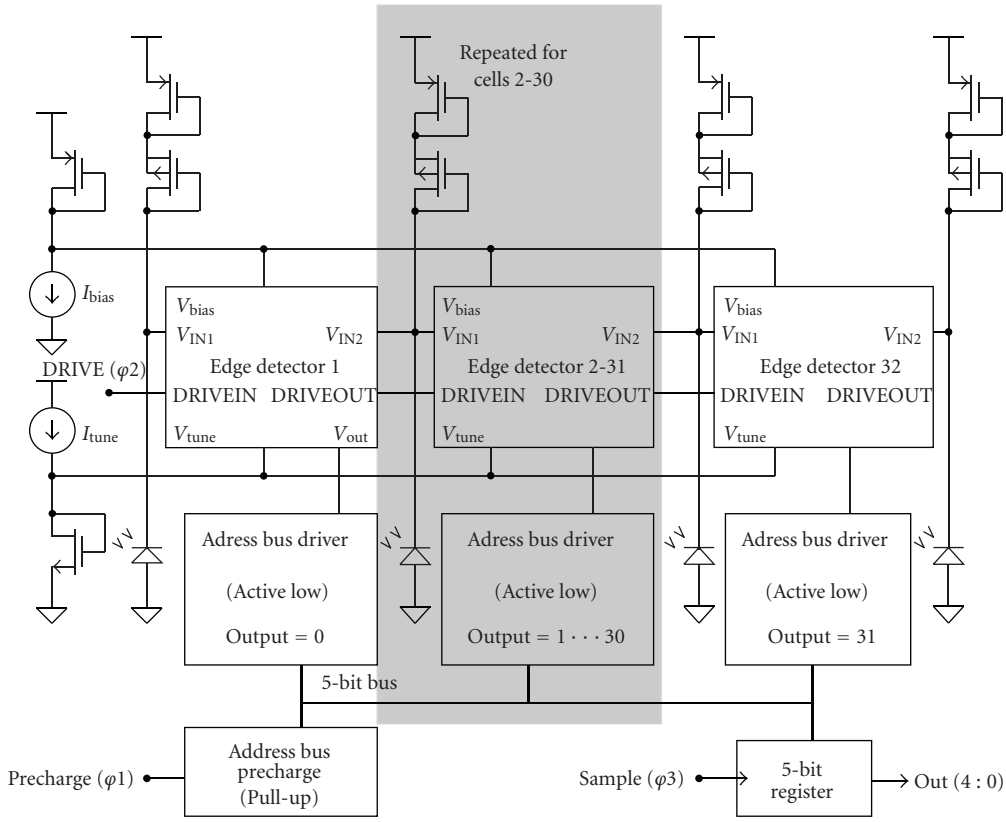

Figure 3: Circuit schematic for the half-plane horizon detector. Each side of the tilt detector uses this horizon detector—comprising of 33 photodetector elements, and 32 edge detector cells—sequentially interrogated until the horizon (i.e., edge) is detected. The address is then asserted onto a precharged bus to encode a digital position output. The shaded region is repeated so as to form a 32-element array.

envisaged that if the nonuniformity of incident light in addition to any component mismatch due to technology variation is maintained to be within the tunable limits, then relatively low bias current levels can be used (i.e., I_{bias} = 5 to 10 nA).

A top-level transient simulation illustrates the system-level operation of the tilt sensor, presented in Figure 10. This simulation assumes an average photocurrent I_{photo} of 25 nA, an ambient *off-current* of 1 nA, and uses a system clock of 500 kHz. The total power consumption is 33 μW.

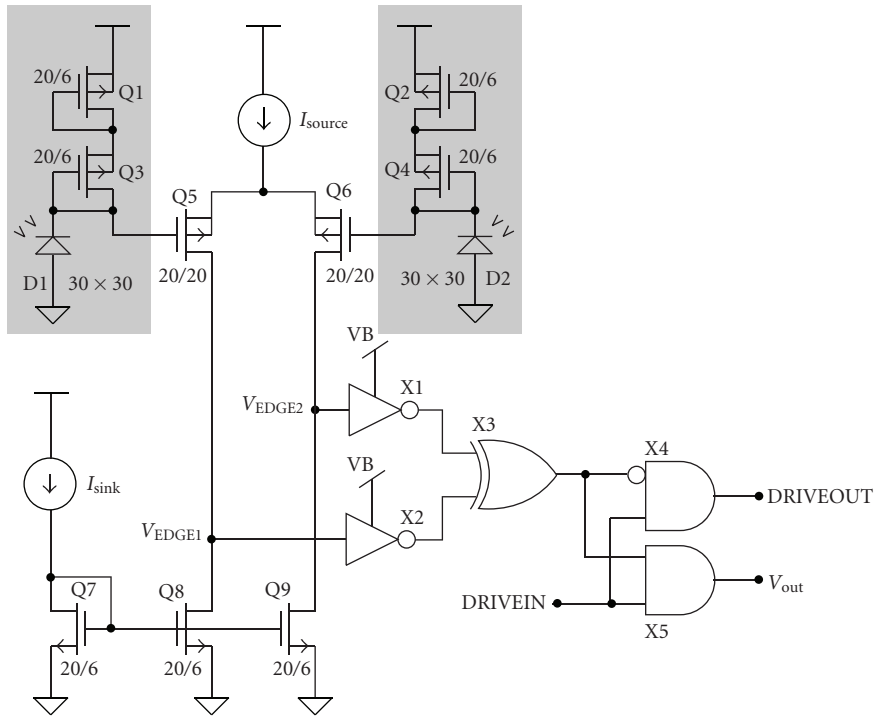

Figure 4: Circuit schematic for the edge detector element. The shaded regions (photodiodes D1-D2 and load devices Q1-Q4) are external to the edge detector block.

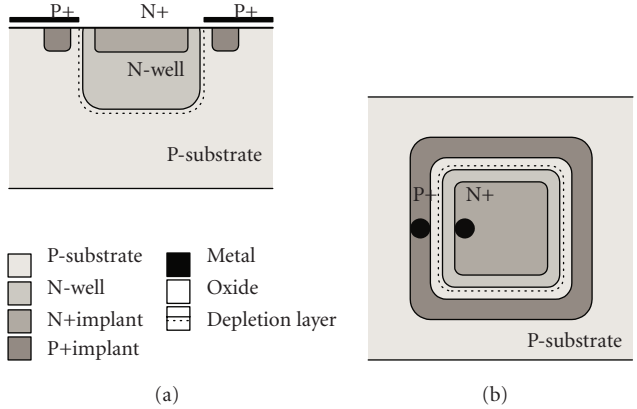

Figure 5: Structure of n-well/p-substrate photodiode showing (a) side, and (b) plan view (not shown to scale or profile).

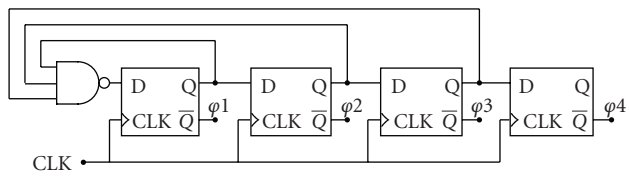

Figure 6: Circuit schematic for the 4-phase clock generation used to sequence actions required to sense the tilt angle.

The functioning of the system can easily be traced by following the transient simulation results shown in Figure 10 as follows: (i) on the rising edge of $\varphi 1$, the two buses are precharged (result = 31). (ii) On the rising edge of $\varphi 2$, the horizon detector results are asserted onto the buses (results of 9 and 14 for LHS and RHS, resp.). (iii) On the rising edge of $\varphi 3$, the values on the buses are sampled to the horizon output registers and finally, (iv) on the rising edge of $\varphi 4$, the subtracted result (from asynchronous adder) is sampled on the output register.

9. DISCUSSION

One aspect of the sensor that has been omitted from the scope of this p is the light source. To ensure robustness in dark and fluctuating light conditions, the sensor is envisaged to incorporate a dedicated light source. This can be a small area, focused (i.e., narrow viewing area) light-emitting diode (LED) to stimulate the photodetectors within the vision chip. The composite emitter/sensor can then be packaged (e.g., as in optoisolators) to seal the components from environmental exposure.

Assuming a typically red (GaAsP) LED has a forward bias of 2 V and the current is limited to 1 mA, the emitter power consumption is 2 mW. For a 2 mm^2 area emitter with 1 mm emitter/sensor separation, a 15° beam divergence and 5% luminous efficiency, this equates to 28 $\mu W/mm^2$ incident light power on the CMOS surface. Therefore, for a photodiode responsivity of approximately 0.3 A/W (at λ = 630 nm), and photodiode area of 4245 μm^2, the generated photocurrent in each illuminated segment will be

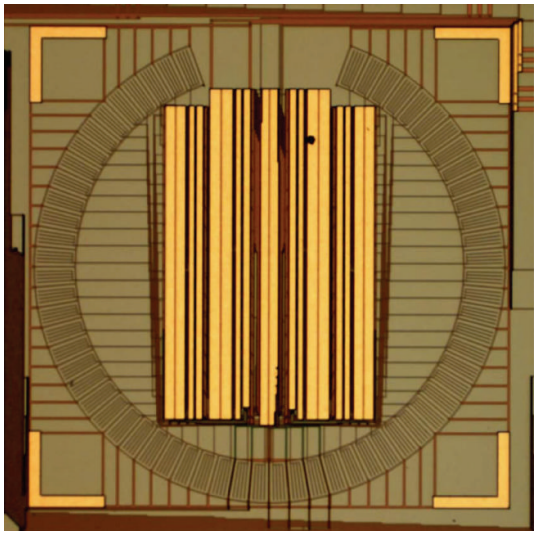

Figure 7: Microphotograph of the tilt sensor electronics implemented in AMS 0.35 μm 2P4M CMOS technology. The dimensions are: 1250 μm × 1250 μm (for core), and 2.5 mm × 2.5 mm die dimensions, that is, including padring and bondpads (not shown).

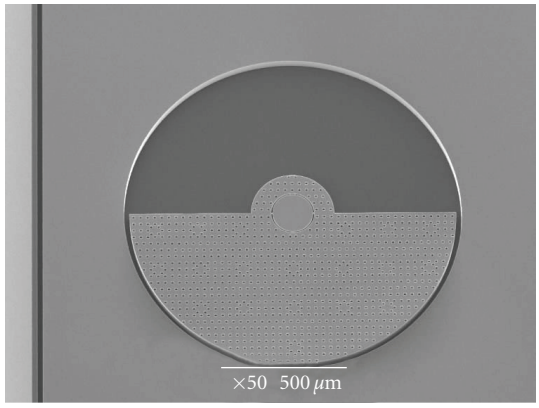

Figure 8: SEM photograph of the micromechanical section of the tilt sensor implemented in the Tronics SOI/HARM technology. The dimensions are: 2.0 mm × 2.0 mm.

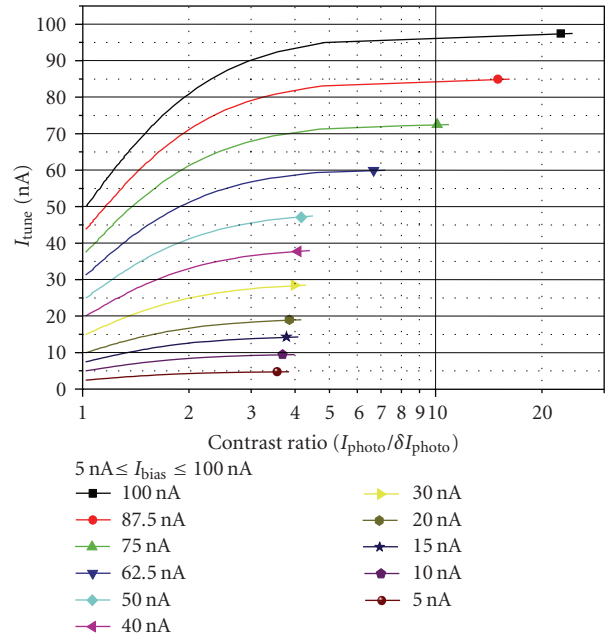

Figure 9: Operational range (for the onset of edge detection) for the edge detector core for various bias conditions (assuming $I_{\text{photo, on}}$ = 25 nA).

Table 1: Target design specifications.

CMOS technology	AMS 0.35 μm 2P4M CMOS
MEMS technology	Tronics SOI/HARM
Supply voltage	3.3 V
Circuit size	2500 μm × 2500 μm
Device count	4312
Input light intensity (range)	10 nW/mm^2 to 100 μW/mm^2
Input system clock (range)	100 Hz to 1 MHz
Input current bias (range)	1 nA to 50 nA
Tilt angle range	330° (±165°)
Tilt resolution	5°
Effective dynamic range	36 dB (6 bits)
System power consumption	†10–35 μW

† Excluding light emitter consumption.

36 nA, well within the operating range of the edge detector [9].

To minimise power consumption, the light source can be biased at reduced intensity as the photodetectors cover a large sense area and is therefore extremely efficient. Alternatively the sensor can be chosen to operate to a duty cycle, that is, pulsing the emitter in synchronisation with the clock, and choosing to power the emitter only at the required refresh rate. For example, if only a 10 Hz tilt response is required, the sensor can be configured to operate for a single acquisition, that is, for four clock cycles (400 microseconds using a 10 kHz clock), every 100 milliseconds, thus reducing power consumption by 99.6%. Fundamentally, the minimum power consumption is only limited by: (i) the dark current of the photodiodes, (ii) the minimum detectable contrast ratio (for reliable edge detection), and (iii) the required sensory response time.

10. CONCLUSION

In this paper, we have presented a hybrid CMOS/MEMS inclinometer that uses a photodetector array to detect the position of a suspended microsystem. With a uniform array of radially positioned photodiodes, the tilt sensor achieves a 5° resolution over a 330° range. The system power consumption depends highly on the incident light intensity but expected to be within the range 10–35 μW. The target system specifications are given in Table 1.

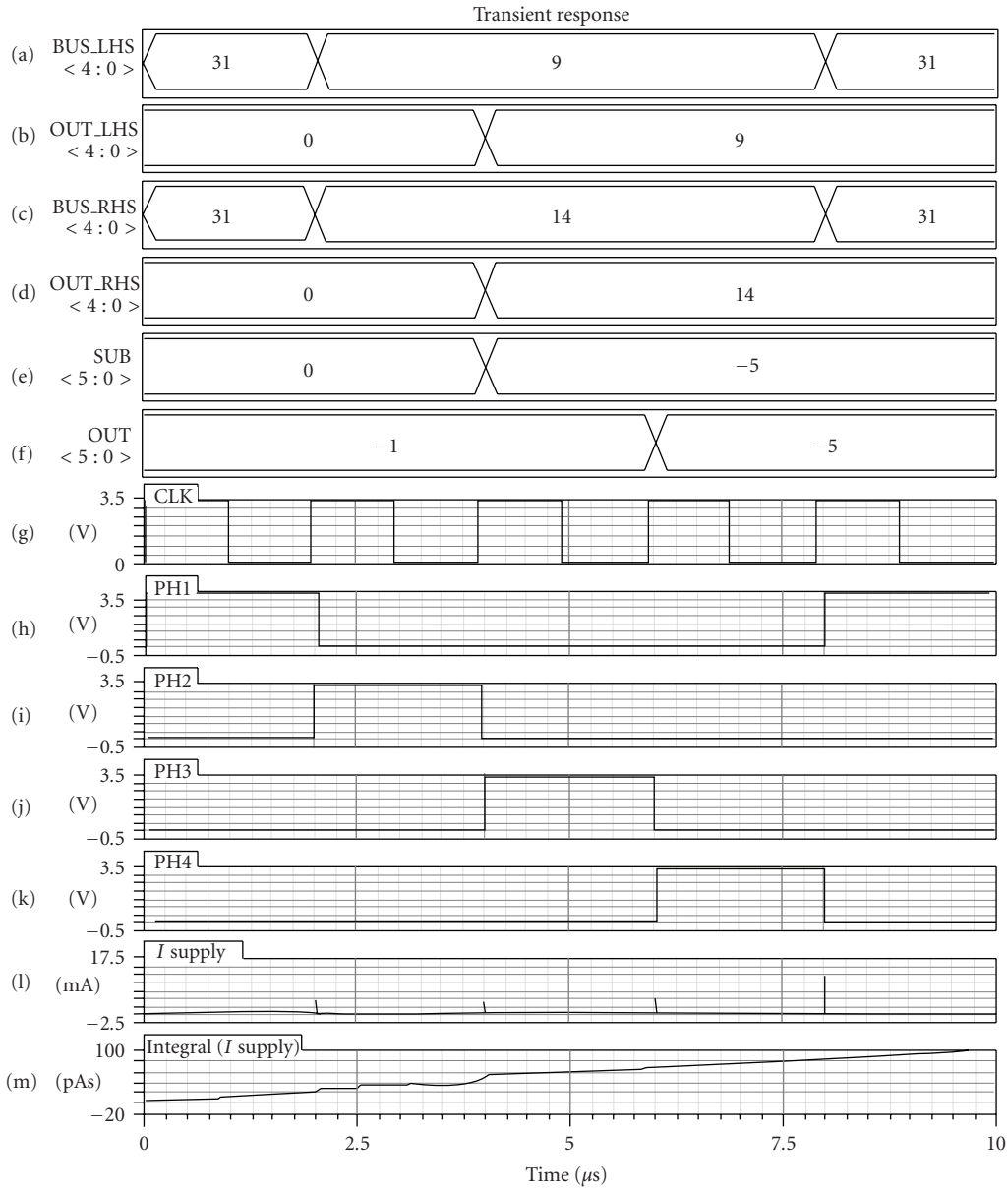

Figure 10: Top-level transient simulation for a tilt angle of −15°. Results shown are (a) LHS horizon bus (5-bit), (b) LHS horizon output (5-bit), (c) RHS horizon bus (5-bit), (d) RHS horizon output (5-bit), (e) subtraction result (6-bit), (f) final output (6-bit), (g) clock, (h)–(k) $\varphi 1$–$\varphi 4$, (l) current supply, and (m) integral of current supply.

ACKNOWLEDGMENT

This work was supported by the Cyprus Research Promotion Foundation (RPF) Grant no. ΠΔΕ-0505/07.

REFERENCES

[1] T. Bretterklieber, H. Zangl, and G. Brasseur, "Impacts on the accuracy of a capacitive inclination sensor," in *Proceedings of the 21st IEEE Instrumentation and Measurement Technology Conference (IMTC '04)*, vol. 3, pp. 2315–2319, Como, Italy, May 2004.

[2] R. A. Yotter, R. R. Baxter, S. Ohno, S. D. Hawley, and D. M. Wilson, "On a micromachined fluidic inclinometer," in *Proceedings of the 12th IEEE International Conference on Transducers, Solid-State Sensors, Actuators and Microsystems*, vol. 2, pp. 1279–1282, Boston, Mass, USA, June 2003.

[3] I.-S. Kang, H. Jung, D.-S. Kim, et al., "Design and fabrication of a MEMS-based electrolytic tilt sensor," in *Proceedings of the International Microprocesses and Nanotechnology Conference*, pp. 216–217, Tokyo, Japan, October 2005.

[4] L. Zhao and E. Yeatman, "Micro capacitive tilt sensor for human body movement detection," in *Proceedings of the 4th International Workshop on Wearable and Implantable Body Sensor Networks (BSN '07)*, vol. 13, pp. 195–200, Aachen, Germany, March 2007.

[5] D. Lapadatu, S. Habibi, B. Reppen, G. Salomonsen, and T. Kvisteroy, "Dual-axes capacitive inclinometer/low-g

accelerometer for automotive applications," in *Proceedings of the 14th IEEE International Conference on Micro Electro Mechanical Systems (MEMS '01)*, pp. 34–37, Interlaken, Switzerland, January 2001.

[6] S. Luczak, W. Oleksiuk, and M. Bodnicki, "Sensing tilt with MEMS accelerometers," *IEEE Sensors Journal*, vol. 6, no. 6, pp. 1669–1675, 2006.

[7] S. Billat, H. Glosch, M. Kunze, et al., "Convection-based micromachined inclinometer using SOI technology," in *Proceedings of the 14th IEEE International Conference on Micro Electro Mechanical Systems (MEMS '01)*, pp. 159–161, Interlaken, Switzerland, January 2001.

[8] N. C. Tien, "Micro-optical inertial sensors using silicon MEMS," in *Proceedings of the IEEE Aerospace Conference*, vol. 1, pp. 437–443, Snowmass, Colo, USA, March 1998.

[9] T. G. Constandinou, J. Georgiou, and C. Toumazou, "Nano-power mixed-signal tunable edge-detection circuit for pixel-level processing in next generation vision systems," *Electronics Letters*, vol. 39, no. 25, pp. 1774–1776, 2003.

[10] T. G. Constandinou and C. Toumazou, "A micropower centroiding vision processor," *IEEE Journal of Solid-State Circuits*, vol. 41, no. 6, pp. 1430–1443, 2006.

[11] Y. Zhao, "Stiction and anti-stiction in MEMS and NEMS," *Acta Mechanica Sinica*, vol. 19, no. 1, pp. 1–10, 2003.